High Voltage

*Research Article*

IET Journals
The Institution of Engineering and Technology

# Development and pattern identification of end-winding discharge under effect of relative humidity and temperature for HV motors

eISSN 2397-7264
Received on 1st June 2019
Revised 5th September 2019
Accepted on 29th October 2019
E-First on 25th February 2020
doi: 10.1049/hve.2019.0124
www.ietdl.org

*Ailiang Kang[1] ✉, Muqin Tian[1], Chuanyang Li[2], Jiancheng Song[1], Simone Vincenzo Suraci[2], Wei Li[1], Lingyan Lin[1], Zhipeng Lei[1], Davide Fabiani[2]*

[1]*Shanxi Key Laboratory of Mining Electrical Equipment and Intelligent Control, College of Electrical and Power Engineering, Taiyuan University of Technology, Taiyuan 030024, People's Republic of China*

[2]*Department of Electrical, Electronic, and Information Engineering 'Guglielmo Marconi', University of Bologna, Viale Risorgimento 2, Bologna 40136, Italy*

✉ *E-mail: kalhyh@qq.com*

**Abstract:** During operation of high voltage (HV) motors, different types of discharges, e.g. surface discharge, corona discharge and bar-to-bar discharge can occur at the same time, increasing the difficulty of partial discharge (PD) sources determination and PDs pattern identification. In this study, the end-winding of a 10 kV motor coil was artificially aged and the related PD was measured. The initiation and variation of different PDs under multi-factor stresses were studied. The localised fingerprints coexisting with multiple PDs were identified and analysed. The results confirm that the end-winding discharge process was significantly influenced by the experiment relative humidity (RH) and temperature. The bar-to-bar discharge was easily recognised at a lower voltage since the identification of bar-to-bar discharge pattern would be affected by the corona discharge pattern at a higher voltage. It is shown that it is more difficult for the corona discharge to be detected when RH exceeded 80%, while the surface discharge dominated at the higher RH. In addition, the PDs were more easily identified with the rise of the temperature. This study can provide a reference in PD identification test and be useful for the PD online monitoring of HV motors.

## 1 Introduction

High voltage (HV) motors are considered as one of the most important electrical equipment, and their failures can lead to serious economic and environmental consequences. Surveys indicate that 37% of their failures are caused by insulation fault occurring in stator windings [1]. In most of the cases, partial discharge (PD) is reported as one of the main reasons leading to the insulation degradation of stator windings even if the mica and glass are PD-resistant [2].

For the insulation inside HV motors, the end-winding insulation can be one of the most vulnerable components, partly because: (i) it suffers because of more complex outer stresses; (ii) the insulation of end-winding is handcrafted, as a result, the electrical and mechanical uniformity cannot be guaranteed. In general, there are three most common types of end-winding discharges: surface discharge, bar-to-bar discharge and corona discharge. These discharges can be electrical natural, even though the initial cause may be not. For instance, the end-winding vibration, which is a typical mechanical problem, can lead to rubbing against coils and inadequate end-winding spacing, causing bar-to-bar discharge if the full phase-to-phase voltage is across adjacent windings [3]. Usually, this mechanism is easy to be spotted in a visual inspection of the end-winding. Intense white powder formation due to ozone will occur between the end-windings. Stone and Wu [4] conducted in-depth studies on this topic. However, non-professionals cannot easily understand why the white powder is produced and what the white powder means despite the visual inspection. Consequently, the end-winding discharges have not received enough attention and could eventually result in the ground and/or phase-to-phase fault.

In recent years, much attention has been paid to PD identification and analysis of PD characteristics by extracting features from the phase-resolved PD (PRPD) patterns [5–11]. However, it is not uncommon that multiple PD sources may exist simultaneously in stator windings, especially in the old non-global vacuum pressure impregnation windings. As a result, a complex PRPD pattern can contain information of features of several types of PD. The identification of complex PRPD patterns into sub-classes corresponding to individual sources is vitally important for accurate PD information interpretation [12].

The general method for pattern identification of multi-source PD is to extract some representative characteristic parameters from PD pulses and apply those to PD quantification [13]. The problem of recognising two active PD sources was solved in [14] by using fractal-based autonomous PD pattern recognition method. The interpretation of the known characteristic of PRPD patterns of specific discharge sources in [15] provides a basis for understanding the development and pattern identification of multi-source PD. Moreover, the experimental conditions also have an impact on the PD development process and pattern identification [16, 17], which might lead to mistakes for PD interpretation.

The scope of this paper mainly focuses on the interpretation of PD development process and pattern identification of multiple simultaneous PD sources. The experiments were carried out in an electromagnetic shielding room under well-controlled conditions. This study could help the development of PD recognition and PD monitoring for HV motors under different relative humidity (RH) and temperature.

## 2 Experimental description

### 2.1 Experimental coils

In this paper, several new 10 kV (phase-to-phase) F-class modern epoxy-mica insulation system stator coils, with the ground-wall insulation thickness of 2.04 mm, were used and tested. The coils were subjected to visual observation before the experiment to ensure that the surface imperfection was non-existent and the semi-conductive coating/stress grading paints were in perfect condition. After that, a 50 Hz voltage was applied across each coil and gradually increased to 15 kV, in order to detect pre-existing internal defects by observing whether only typical symmetrical PRPD patterns of internal discharge occurrence [18].



This is an open access article published by the IET and CEPRI under the Creative Commons Attribution License (http://creativecommons.org/licenses/by/3.0/)

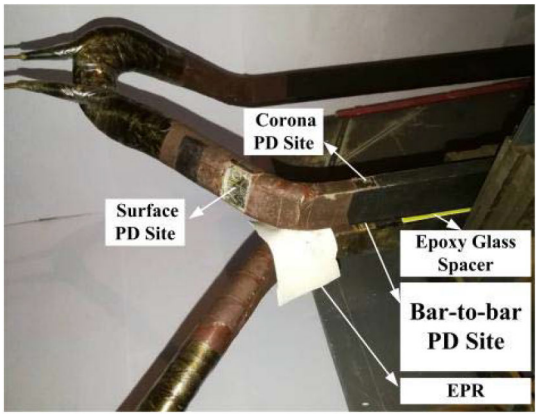


**Fig. 1** *Photo of end-winding discharge model*

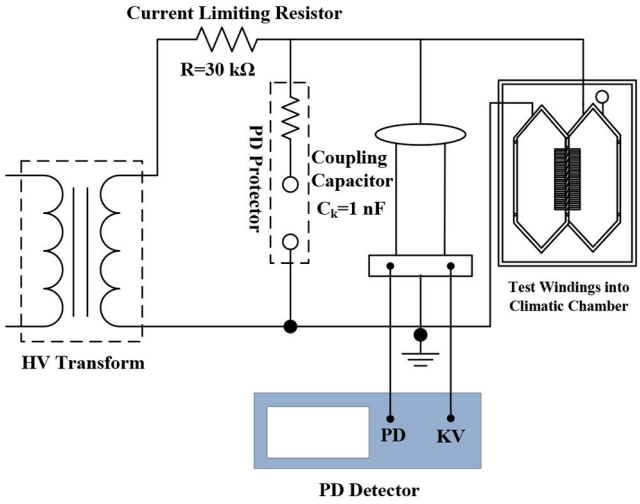


**Fig. 2** *Experiment schematic diagram of PDs measurement system*

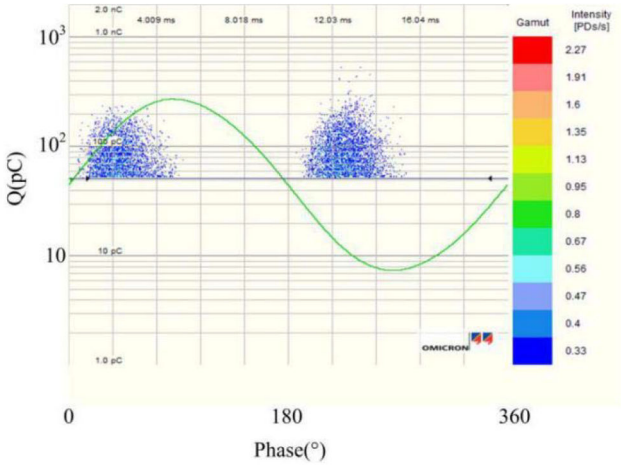


**Fig. 3** *PRPD pattern of internal discharge measured at 20°C and RH of 40% under the voltage of 10 kV*

### 2.2 Experimental set-up

In this paper, an experimental model with three types of end-winding discharge was made, as shown in Fig. 1. The model contained two stator coils, and the junction of semiconductor and stress grading paints of two coils was abraded to induce corona discharge; at the same time, the end arms of two coils were abraded to induce surface discharge; the distance of the crossover of the end-arm between top and bottom coils was adjusted to 3 mm in order to induce bar-to-bar discharge [15]. The function of the epoxy glass spacer and EPR shown in Fig. 1 was to restrain other PD activities. All tests were carried out at both room temperature (20°C) and HV motors operating temperature (80°C), respectively.

**Table 1** Experimental conditions

| RH | $V_{age}$, kV | $T$, °C | $T_c$, °C |
|---|---|---|---|
| 40–95% | 15 | 20 | 20 |
| | | 80 | |

It is worth noting that 80°C was the temperature of the surface of the insulation.

The experiment was performed in a climatic chamber with a dimension of 150 cm × 50 cm × 50 cm, which can provide constant RH and temperature. The neutral water was put into a humidifier with the vibration frequency of 500 kHz, which could ensure the diameter of vapours around 10 μm. The experimental details are shown in Table 1. $V_{age}$ is the ageing voltage, $T_c$ is the temperature in the climatic chamber, $T$ is the temperature of the PD site. The highest considered temperature, 80°C, is not considered to be an accelerating ageing factor but could accelerate the discharge activity with respect to the condition of room temperature.

### 2.3 PD measurements

The schematic diagram of the PD acquisition system used for the study is shown in Fig. 2. The AC test voltage is generated by a 50 Hz, 100 kV, 10 kVA test transformer with the PD amplitude of 0.2 pC at 100 kV. A 30 kΩ resistor is used as a current limiter. The PD protector is made up of a water resistor and a copper ball.

In order to monitor the evolution of end-winding discharge activity and understand how the experiment conditions influence PD activity and PD distribution, PRPD patterns were recorded during the experiment process. To obtain stable PRPD patterns under different temperatures and RH, all experimental stator coils were annealed at 20°C and RH of 40% under the voltage of 6 kV for 4 h before the experiment. After that, these coils were connected to a 15 kV source for 24 h under different RH and temperature. The PD measurements were performed under the application of an increasing AC voltage, in the form of step voltage increases, so the PD development process and each type of PD could be observed in detail. PRPD patterns were recorded with a 1 nF capacitive coupler in a frequency of 0.1–20 MHz for 2 min.

## 3 Results

### 3.1 PRPD patterns

The PRPD pattern contains not only information about the interpretation of the PD activity caused by the physical process, but also about its position with respect to the electrode (symmetrical or asymmetrical PD-signal clusters) [19].

The internal discharge is always unavoidable in HV motors and there is no damage to the insulation under operating conditions. The PRPD patterns of internal discharge are characterised by symmetry in the maximum amplitude and in the number of discharge pulses in both voltage half cycles, and the $Q_{peak}$ of this type of discharge is about 300 pC at 10 kV, as shown in Fig. 3.

Fig. 4 shows the end-winding discharge development process and the corresponding PRPD pattern measured at 20°C and RH of 40% under 7.0, 8.0, 9.0 and 13.0 kV, respectively. When the voltage is 7.0 kV, bar-to-bar discharge can be observed clearly, as shown in Fig. 4*a*. The PRPD pattern of bar-to-bar discharge is characterised by symmetry with almost constant amplitude in both voltage half cycles, it is a typical gap discharge with much larger air gap spacing than for internal discharge occurring in minute voids into the insulation [17]. When the voltage is up to 8.0 kV, the corona discharge occurs and the PRPD pattern shows prominently asymmetry with much larger amplitude in the negative voltage half cycle. When the voltage is further up to 9.0 kV, surface discharge can be detected, and the PRPD pattern is somewhat like 'rabbit ear'. The reason for this is that water vapour in air covers on the voids or cavities of the end-winding surface, resulting in the typical PD pattern of a void or cavity superimposed with a surface discharge inside the void [19].

When the RH of the climatic chamber is 60%, the PRPD patterns have a great difference compared with the patterns


This is an open access article published by the IET and CEPRI under the Creative Commons Attribution License (http://creativecommons.org/licenses/by/3.0/)

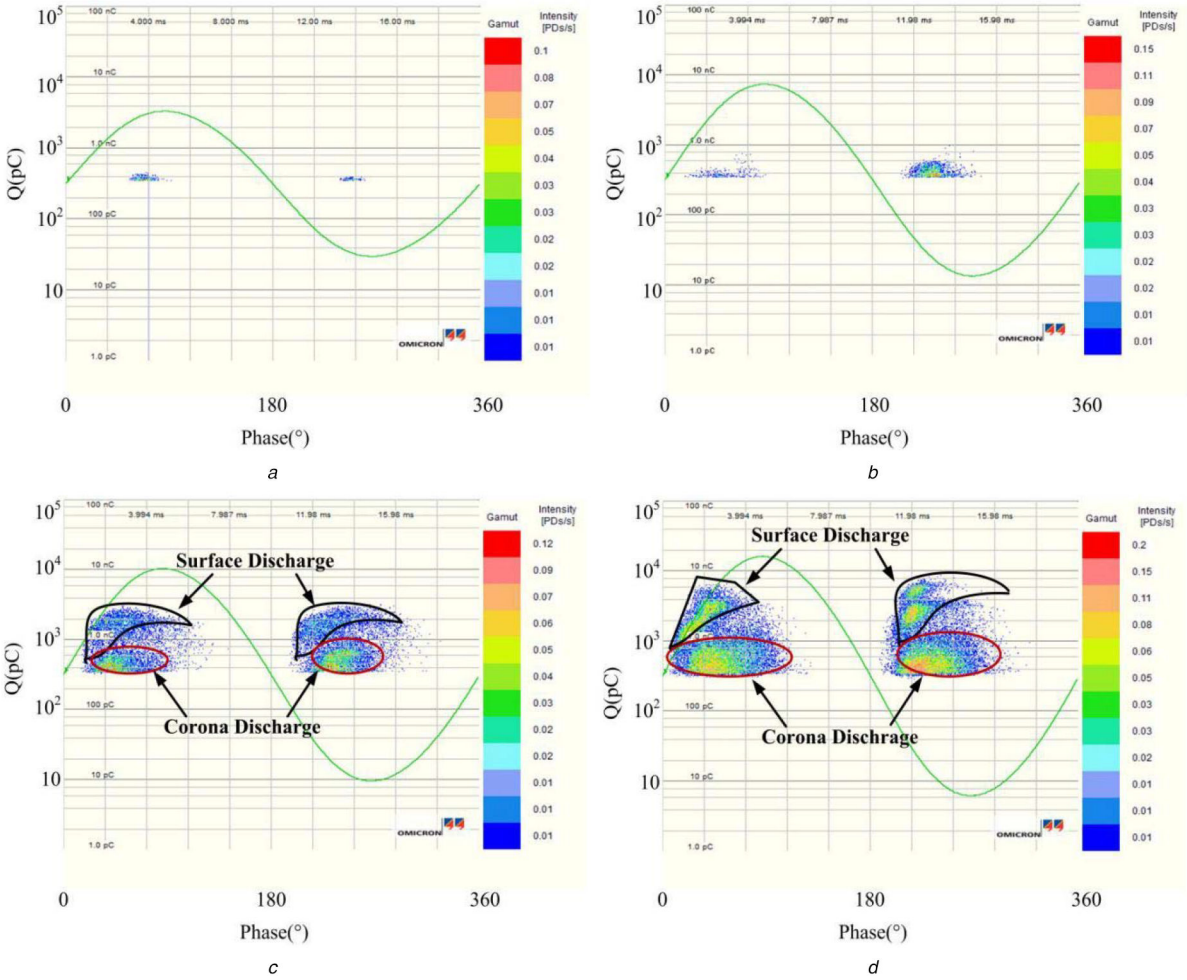


**Fig. 4** *PRPD patterns measured at 20°C and RH of 40% under the voltage* ***(a)*** 7.0 kV, ***(b)*** 8.0 kV, ***(c)*** 9.0 kV, ***(d)*** 13.0 kV

measured under RH of 40%, as shown in Fig. 5. The bar-to-bar discharge can be detected until 8.0 kV with the $Q_{peak}$ of about 591 pC. The corona discharge can be observed until 10.0 kV and the PRPD pattern becomes symmetrical because of the increase of RH, as shown in Fig. 5*b*. More remarkable, the surface discharge activity is intense when the voltage is up to 12.0 kV, and the predominant feature of its PRPD pattern is that it gives rise to a few very large discharges with the $Q_{peak}$ as high as 10 nC in the negative voltage half cycle, as shown in Figs. 5*c* and *d*. Besides, when the voltage is higher than 9.0 kV, the bar-to-bar discharge is completely drowned out by the corona discharge, and we cannot directly identify them from the complex PRPD pattern, however, the surface discharge can be easily recognised, as shown in Figs. 5*c* and *d*.

It can be seen from Fig. 6 that the discharge is more difficult to induce when the RH is equal or higher than 95%. The bar-to-bar discharge occurs when the voltage is 8.0 kV but with much less discharge pulses, and the $Q_{peak}$ is much lower than those at the condition of 40 and 60%. Besides, the surface discharge and 'rabbit ear' pattern can be observed until the voltage is increased to 13.0 kV.

Fig. 7 shows PRPD patterns recorded at 80°C and RH of 60% under different voltages. It can be clearly seen that the surface discharge occurs at 5.0 kV, the bar-to-bar discharge and corona discharge are detected at 6.0 and 8.0 kV, respectively. Meanwhile, the $Q_{peak}$ and the number of discharges are much higher than those at 20°C and RH of 60%. Besides, when the voltage is higher than 10.0 kV, the PRPD patterns are made up of the three types of end-winding discharges, and the bar-to-bar discharge and corona discharge are too superimposed to identify each other. Fortunately, the surface discharge can be recognised from the complex PRPD pattern just through visual inspection, as shown in the oval portions in Figs. 7*b* and *d*. Furthermore, the surface discharge magnitude is the highest among the three types of end-winding discharges, resulting in bigger damage to the end-winding insulation.

### *3.2 Discharge parameters distribution*

As depicted in Fig. 8, the DIV (discharge inception voltage) measured at 80°C is much lower than the one measured at 20°C. Besides, in the case of the two curves, the DIV shows a slow growth between RH = 40% and RH = 70%, and then hugely increases when RH exceeds 70%. However, the DIV measured at 20°C fluctuates very imperceptibly between RH = 80% and RH = 95%, while this phenomenon does not happen at 80°C. Furthermore, there is a linear relationship between the DIV and the experimental RH, and the linear fitting parameters are shown in Table 2. From which we can know that the linear fit at 20°C is much better than the one at 80°C. It should be pointed out that the higher temperature can promote the end-winding discharge and accordingly decrease the DIV.

Fig. 9 shows the $Q_{Avg}$ changes with different RH. It can be seen that the curves keep basically the same from 6 to 8 kV at 80°C under RH of 60 and 80%. Besides, the PD amplitudes are scattered over a relatively wide range, and the change of $Q_{peak}$ differs a lot under different RH and temperature. It is very hard to induce end-winding discharge even though the voltage is equal or higher than 6 kV at 20°C, and the $Q_{peak}$ is <4000 pC even at 10 kV. However, the $Q_{peak}$ is much higher and the discharge can be observed at 4 kV when the temperature is up to 80°C. Furthermore, the $Q_{peak}$ decreases with the increase of RH and the attenuation trend is more obviously at 80°C. In addition, when the temperature is 80°C, the difference value of $Q_{Avg}$ under the condition of 80 and 95% is


This is an open access article published by the IET and CEPRI under the Creative Commons Attribution License (http://creativecommons.org/licenses/by/3.0/)

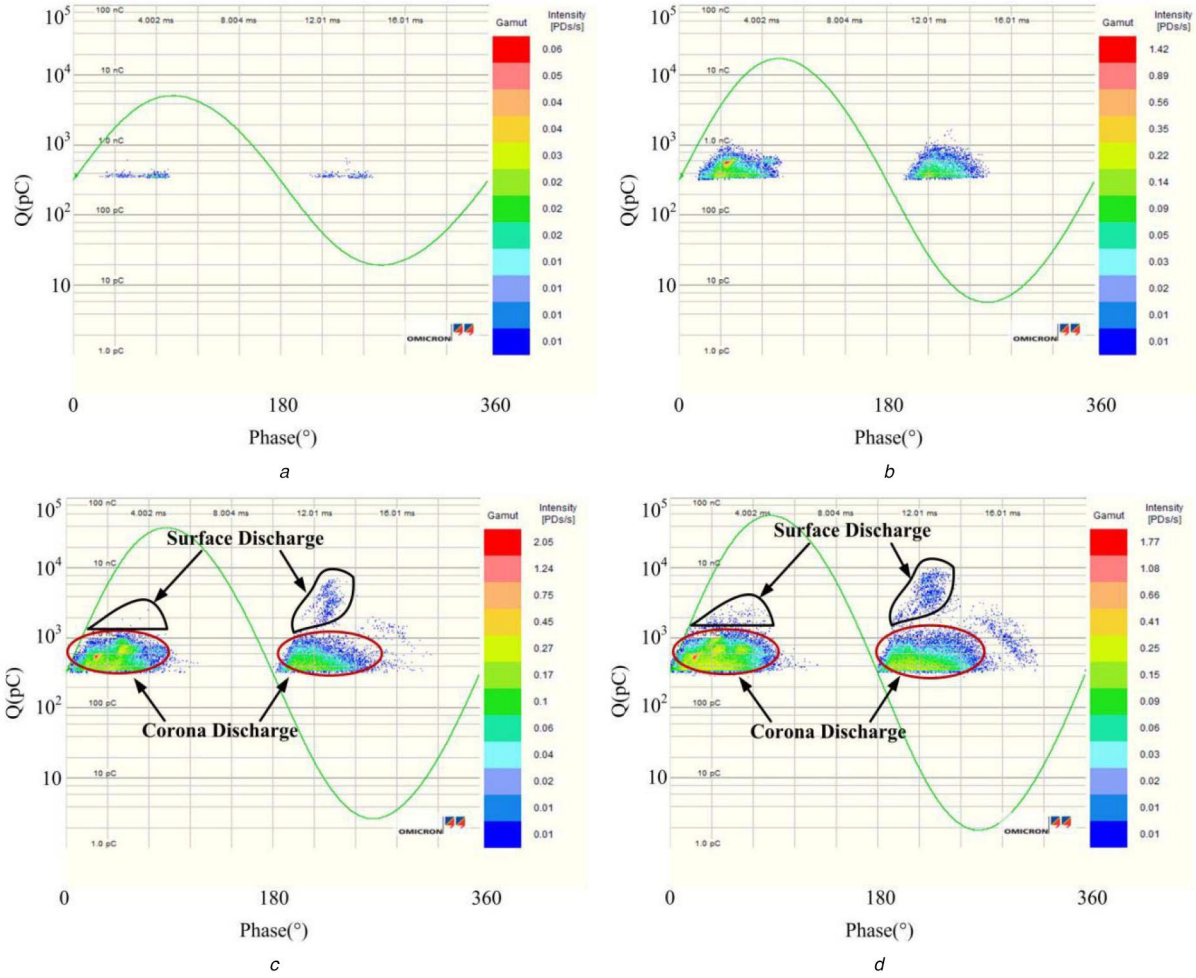


**Fig. 5** *PRPD patterns measured at 20°C and RH of 60% under the voltage* ***(a)*** 8.0 kV, ***(b)*** 10.0 kV, ***(c)*** 12.0 kV, ***(d)*** 13.0 kV

much smaller than $Q_{peak}$, which reveals that low-amplitude discharges are predominant in the PD activity under high RH.

The DRR (discharge repetition rate) is positively correlated with the intensity of discharge activity. As depicted in Fig. 10, the discharge process could be divided into three stages when the temperature is 80°C: (i) When the voltage is lower than 5 kV, the DRR is very low and almost unchanged. (ii) When the voltage is in the range from 5 to 8 kV, the growth trend is slow and the DRR is up to hundreds of PDs/s. (iii) When the voltage is higher than 8 kV, the tendency of DRR increases rapidly, and the DRR is over 1600 PDs/s under the condition of 10 kV, 40% and 80°C. Besides, the DRR changes dramatically until 8 kV at 20°C. Meanwhile, it should be noted that the tendency of the curves becomes subdued and depressed when the RH is from 40 to 95%. However, the DRR under the condition of 20°C and 40% exceeds the one of the 80°C and 95% condition when the voltage is higher than 9 kV, which proves that temperature and RH together determine the intensity of PD activity.

The $P_{Dis}$ (discharge power) characterises $Q$, the DRR and the instantaneous value of applied voltage during discharge, which contains more PD information and estimates the PD activity more comprehensively. As shown in Fig. 11, the trend of the $P_{Dis}$ is decreased with the increase of RH at the same temperature. Besides, the curves under different RH measured at 80°C obviously change, although the difference values of these curves gradually shrink. It is worth commenting that the curves measured at 20°C have a high degree of similarity, except for the condition of 20°C and 40%. Moreover, it is noteworthy that the $P_{Dis}$ measured at the condition of 20°C and 40% equals the one of 80°C and 95% condition when the voltage is 10 kV. The result indicates that PD energy may be the same although the experiment conditions have a great difference.

### *3.3 PD pattern identification*

When the applied voltage is higher than the DIV, the PD will be recorded, and a complex PRPD pattern will generate if the experimental conditions can induce more than one type of discharge. In this paper, the three-frequency (3FREQ) method, which can measure the PDs in three frequency bands simultaneously, is proposed to identify the complex PRPD patterns. As depicted in Fig. 12, the plot on the left shows the PD pulses distribution in 3FREQ diagram, and the plot on the right is the corresponding PRPD patterns of the selected area in the plot on the left. In Fig. 12, three types of end-winding discharges are simultaneously present in a complex PRPD pattern, and the PD pulses are radial with one PD centre (the PD centre is the reddish region in the PRPD pattern, which contains most of the PDs). Consequently, it is very difficult to recognise each of them because the discharges are superimposed. In this paper, we identify each of the three types of discharges, and it is helpful for us to understand the distribution of PDs in the complex PRPD pattern. Fig. 12 shows the PD distribution and identification measured at 20°C and RH of 40% under the voltage of 13.0 kV. Wherein, part A represents only corona discharge, part B is made up of most corona discharge and a little surface discharge, part C is bar-to-bar discharge and part D consists of most surface discharges and a little corona discharge. It should be noted that surface discharge plays a dominant role in the complex PRPD pattern both in the discharge amplitude and the number of discharges.

In the experiment, we find that the PD distribution is also affected by the experimental conditions. As previously mentioned, the PDs are drastically attenuated in high humidity conditions, and contextually, the PDs are too superimposed to identify. Fig. 13 shows the PDs separation measured at 20°C, 13 kV and RH of 95%, the PD centre is dispersive at a large area. As for the complex


This is an open access article published by the IET and CEPRI under the Creative Commons Attribution License (http://creativecommons.org/licenses/by/3.0/)

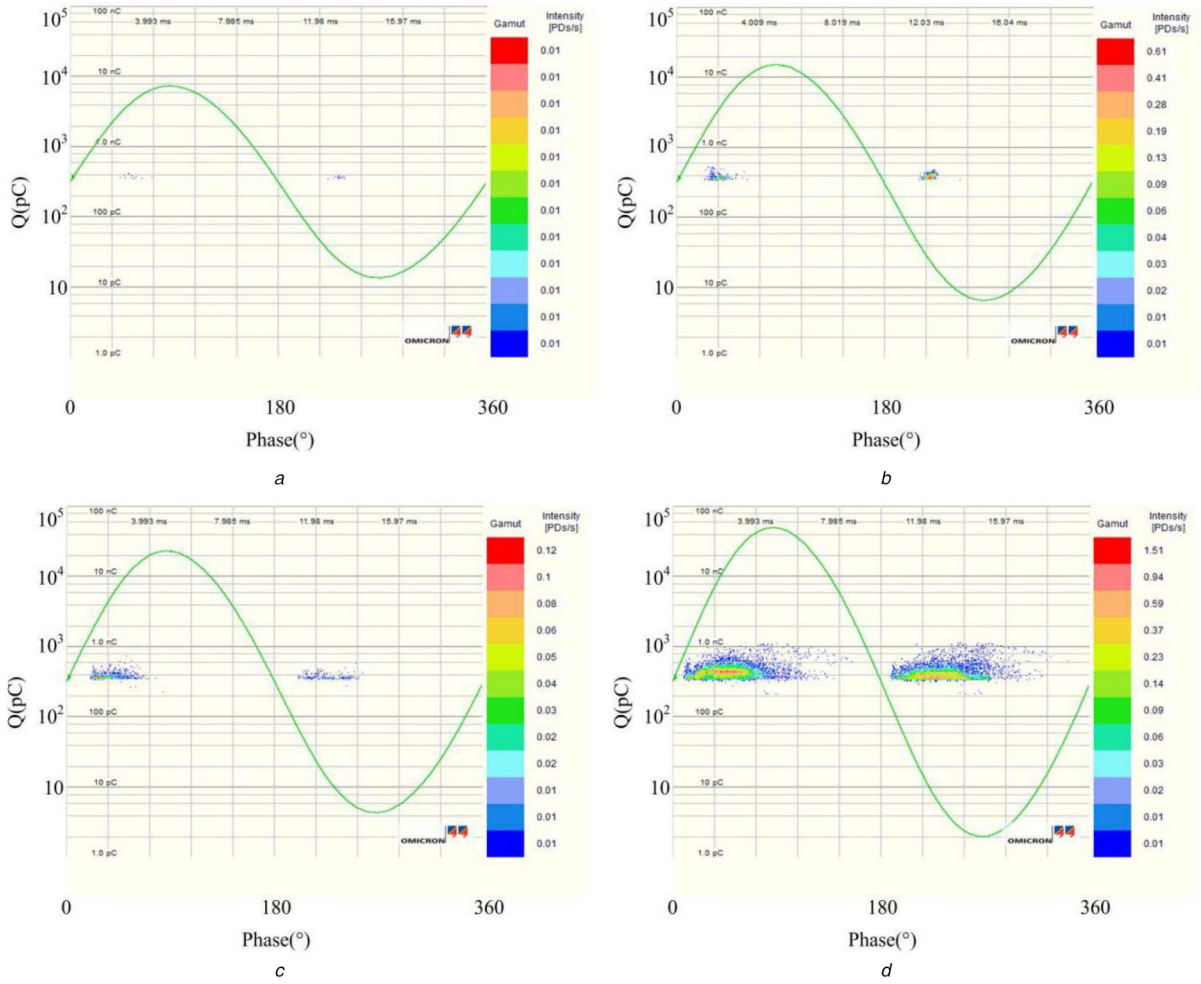


**Fig. 6** *PRPD patterns measured at 20°C and RH of 95% under the voltage* ***(a)*** 8.0 kV, ***(b)*** 10.0 kV, ***(c)*** 11.0 kV, ***(d)*** 13.0 kV

PRPD pattern, the PD separation is more difficult compared to Fig. 12. The four parts are highly similar to bar-to-bar discharge patterns and only part C contains a little surface discharge. On the other hand, the PDs are more easily identifiable at high temperature, as shown in Fig. 14. The complex PRPD pattern consists of two parts, one of which is corona discharge, as depicted in part A. In the complex pattern, we identify two kinds of bar-to-bar discharges with different amplitudes, as shown in part B and part D. The reason is that there are several air gaps with different dimensions, leading to different local fields on the PD site. Meanwhile, surface discharge is also identified in the pattern, as shown in part C.

## 4 Discussion

The PD signal analyses of HV generators and motors have been studied for over 40 years [20]. However, most of them focus on the single type of PD and its characterisation under different conditions. In this paper, the junction section and the end arm of two windings are abraded to induce the three types of PDs. In the experiment, we have found that humidity and temperature around the PD sites play an important role in the PD progress. However, the end-winding discharge is very complex because it contains three types of discharges and these discharges are superposed in some cases, which leads to a very difficult identification of PDs characteristics. This paper analyses the end-winding discharge development and its characterisation with multiple types of PDs, explores the influence of humidity and temperature on the PD progress and finally identifies these PDs in the best possible way.

### *4.1 Influence of temperature on end-winding discharge*

The end-winding discharge is significantly affected by temperature. It has been shown in previous work that oil-contamination surface discharge increased with temperature in very short exposure time to voltage and RH [16]. In our experiment, the influence of temperature is one of the parameters we could isolate, as illustrated in Figs. 5 and 7, where end-winding PDs are measured under the same humidity but at different temperatures, 20°C (Fig. 5) and 80°C (Fig. 7). These patterns clearly show that the intensity of end-winding PDs did increase with temperature and the DIV did decrease from 7.2 kV (20°C) to 4.2 kV (80°C). Besides, Figs. 5*b* and 7*d* are measured at the same voltage (10.0 kV), and their parameters are calculated in Table 3. In Table 3, we can see that all parameters increase significantly with temperature. In Fig. 7*d*, we can clearly observe the presence of corona discharge, bar-to-bar discharge and surface discharge. However, in Fig. 5*b*, surface discharge cannot be observed. In addition, the PRPD patterns of positive voltage polarity and negative voltage polarity are almost symmetrical in Figs. 5*a* and *b*, however, the PRPD patterns show obvious asymmetry from Figs. 7*a–d*. The change of PD patterns can be explained by the increase in the electrons thermal energy, resulting in a more effective ionisation and also a bigger number of initial electrons by photoemission [21].

### *4.2 Influence of RH on end-winding discharge*

Water vapour in the air is a kind of gas with electronegative nature, which can considerably impact the PD process [22, 23]. Therefore, a higher RH leads to a reduction of end-winding discharge activity in our experiment. A further explanation of this phenomenon can be found in our previous work [15].


This is an open access article published by the IET and CEPRI under the Creative Commons Attribution License (http://creativecommons.org/licenses/by/3.0/)

In this study, under the condition of 20°C and 95%, the PRPD patterns result to be symmetrical again when end-winding discharge is subdued. This phenomenon can be explained through the effect of humidity inside the insulation. When the RH is high, the density of water vapour around the end arms will increase sharply. Water molecules will be ionised and aggregated under high

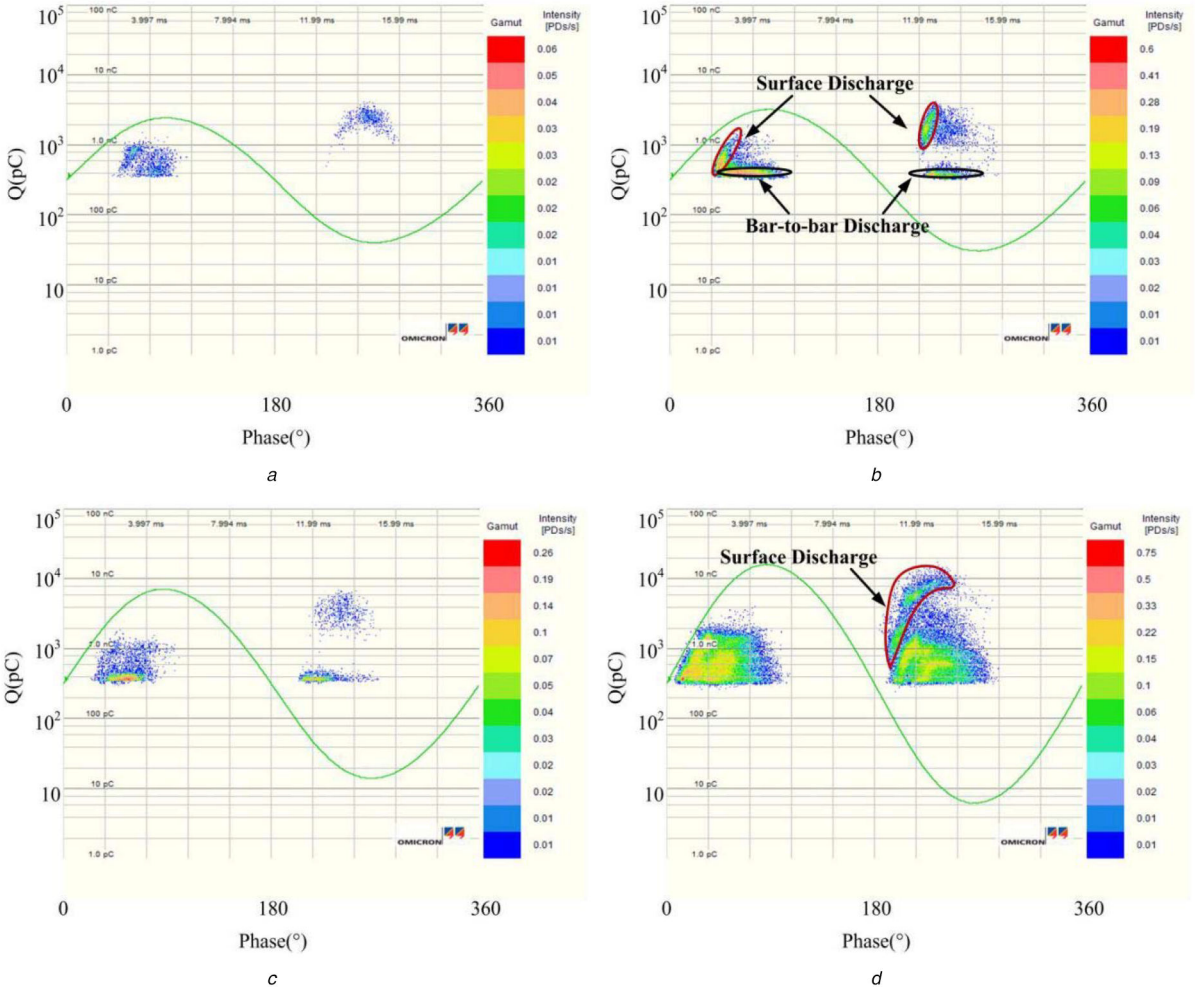


**Fig. 7** *PRPD patterns measured at 80°C and RH of 60% under the voltage*
***(a)*** 5.0 kV, ***(b)*** 6.0 kV, ***(c)*** 8.0 kV, ***(d)*** 10.0 kV

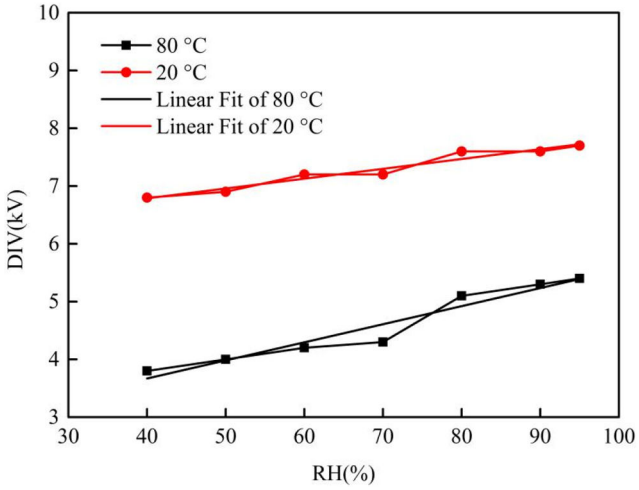


**Fig. 8** *DIV measured under different RH and temperature*

**Table 2** Linear fitting parameters of two DIV curves

| | | Value | Standard error |
|---|---|---|---|
| 20°C | slope | 0.01703 | 0.00173 |
| | intercept | 6.10609 | 0.12421 |
| 80°C | slope | 0.0313 | 0.00354 |
| | intercept | 2.41686 | 0.25421 |


This is an open access article published by the IET and CEPRI under the Creative Commons Attribution License (http://creativecommons.org/licenses/by/3.0/)

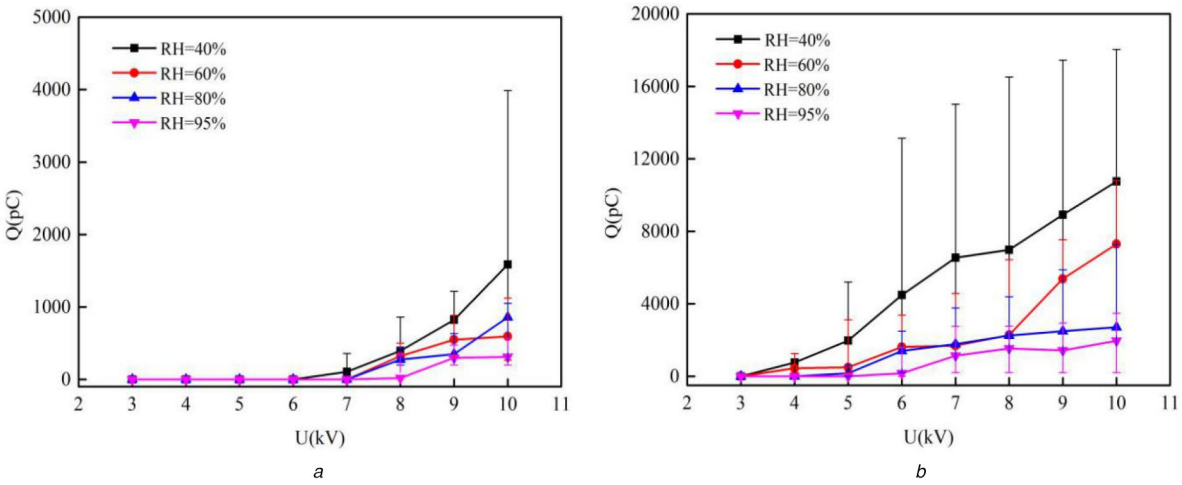


**Fig. 9** *$Q_{Avg}$ changes in the temperature of*
***(a)*** 20°C, ***(b)*** 80°C, with respect to different RH

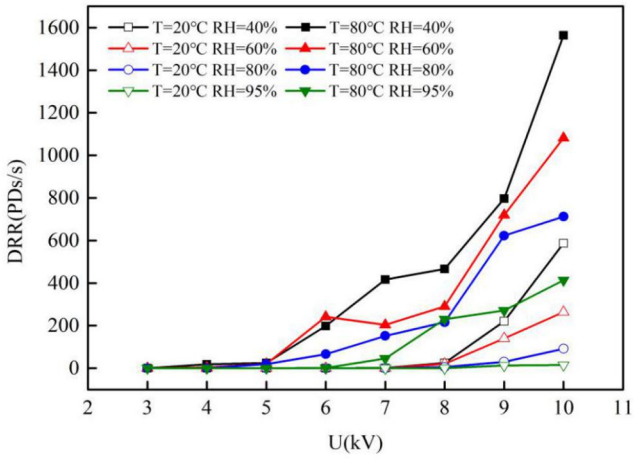


**Fig. 10** *DRR changes with respect to the applied voltage under different RH and temperature*

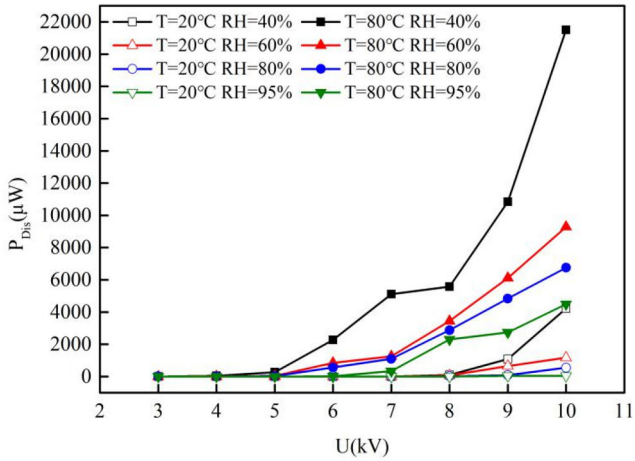


**Fig. 11** *Discharge power changes with respect to the applied voltage under different RH and temperature*

electric field, resulting in heterogeneity of the local field and a reduction of the discharge activity. The nature of this type of PD is gas medium discharge, which has a lower intensity discharge compared with the single gas or solid discharge. The PD parameters gradually decrease with the increase of RH, under the same voltage and temperature, as seen in Table 4. Wherein, the ratio of DRR under different RH is 39.0, in addition, the ratio of $P_{Dis}$ is as high as 88.6. The changes of PD parameters under different RH indicate that humidity can significantly suppress the end-winding discharge. Furthermore, the suppression of PD intensity is more pronounced at 20°C with the increase of RH, because water molecules are able to capture free electrons with lower thermal energy.

In our experiment, we find an interesting phenomenon. The measured PD parameters are very similar under the condition of 20°C, 40%, 10 kV and 80°C, 95%, 10 kV, as shown in Table 5, but the PRPD patterns have a great difference. The ratios of $Q_{peak}$, $Q_{Avg}$ and $P_{Dis}$ are very close to 1.0, except for the ratio of DRR. As a result, the PD intensity is basically the same although the experimental conditions greatly differ. The reason for this is that the acceleration of temperature on the end-winding discharge neutralises the inhibition of RH on the end-winding discharge.


This is an open access article published by the IET and CEPRI under the Creative Commons Attribution License
(http://creativecommons.org/licenses/by/3.0/)

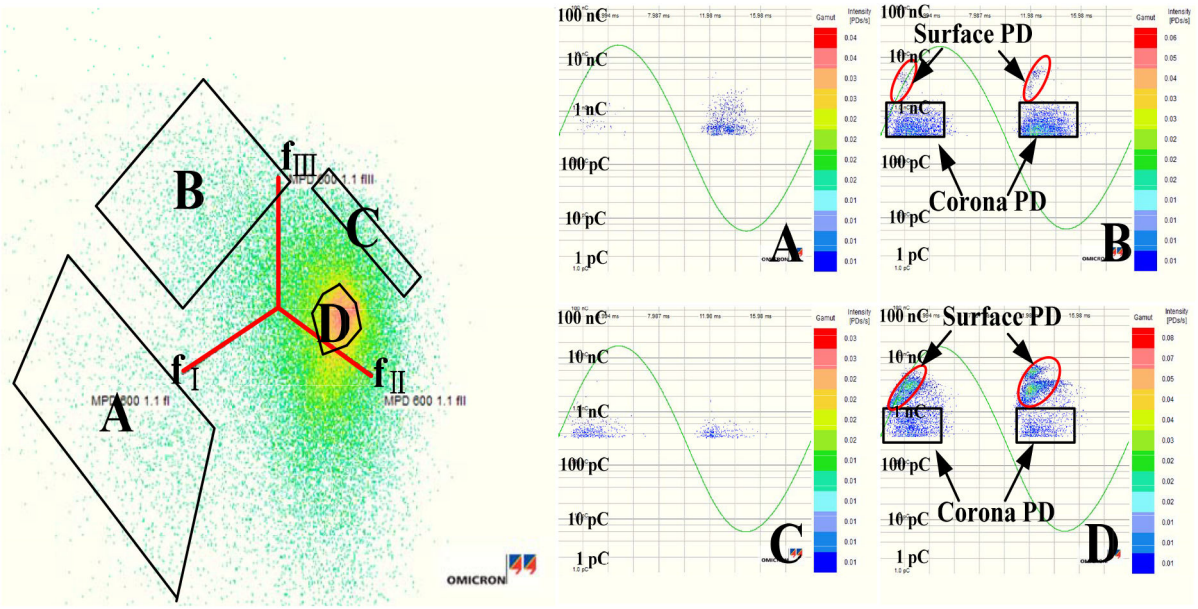


**Fig. 12** *PD distribution and its identification measured at 20°C and RH of 40% under the voltage 13.0 kV*

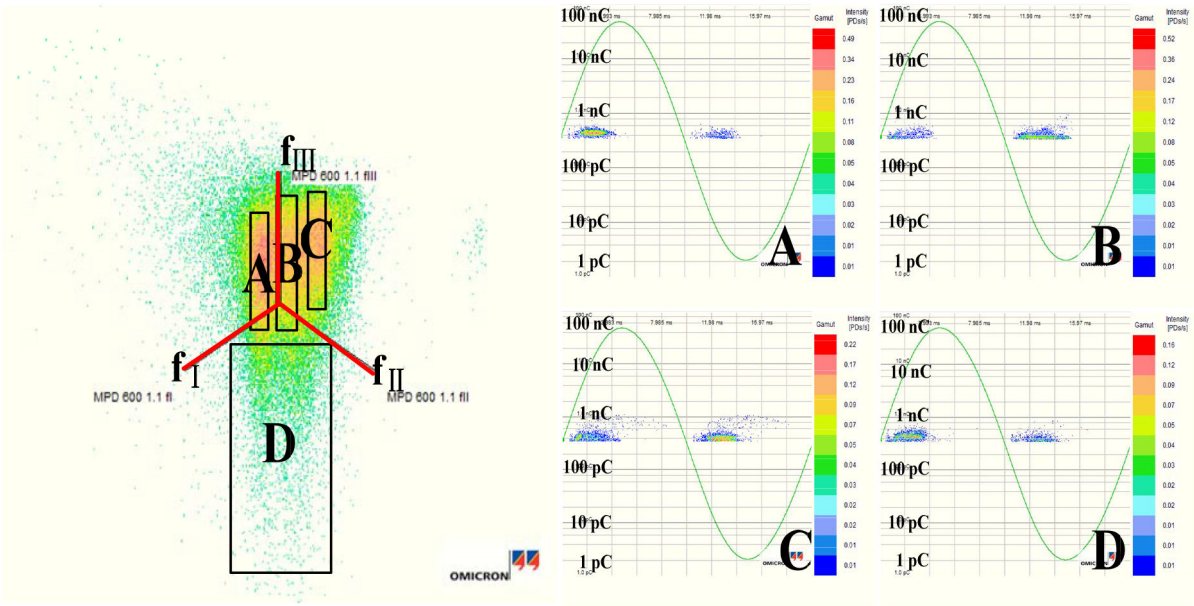


**Fig. 13** *PD distribution and its identification measured at 20°C and RH of 95% under the voltage 13.0 kV*

Consequently, it is very easy to make mistakes, resulting in error warnings if the monitoring system only considers the PD parameters without considering the PRPD patterns.

### *4.3 Influence of temperature and RH on PD identification*

The end-winding discharge contains three of the most common discharges and their DIVs are greatly influenced by the environmental conditions, such as temperature and RH around the PD sites. In our experiment, the bar-to-bar discharge can be observed in any conditions, but the corona discharge will disappear under high RH and room temperature, anyway, surface discharge occurs only at the condition of high RH and/or high voltage. However, due to the limit of the experimental apparatus, most of the discharges are superimposed together and only parts of discharges can be identified clearly. Fortunately, we can still accurately determine what kind of discharge has occurred by comparing the complex PRPD patterns with the separated PDs PRPD patterns, as shown in Figs. 12–14. Among the three most common end-winding discharges, the bar-to-bar discharge can be inspected firstly and there will be more than one bar-to-bar discharge source under certain experiment conditions, as shown in Fig. 13. The reason is that bar-to-bar discharge is strongly related to the local field and the dimension of the air gap. This activity can occur in some large air gaps when the local field exceeds the discharge inception field. Hence, at room temperature and lower voltage, the PD is also present, but much less pronounced and with lower amplitude. Accordingly, the bar-to-bar discharge activity is very intense with higher amplitude at higher voltage and temperature, as shown in Fig. 14. Meanwhile, as previously mentioned, the end-winding discharge can be promoted with the increase of temperature, the PDs are more isolated, and the PD separation is more efficient, as shown in Fig. 14. In another experiment, we conducted the end-winding discharge under electrical-thermal ageing, the PDs were further isolated and PD separation was further efficient, as depicted in Fig. 15. The PDs are identified and the boundaries are pretty clear. Wherein, part A and part C are surface discharges; part B, part D and part E are bar-to-bar discharge. Besides, corona discharges are very rare and superimposed with surface discharge, and we cannot identify it from the complex PRPD pattern.

In addition, the discharge activities are attenuated with the increase of RH, and some PDs would be disappeared or not active, consequently, the PRPD patterns will be difficult to identify, even for experts. In our experiment, when the RH exceeds 80%, corona


This is an open access article published by the IET and CEPRI under the Creative Commons Attribution License (http://creativecommons.org/licenses/by/3.0/)

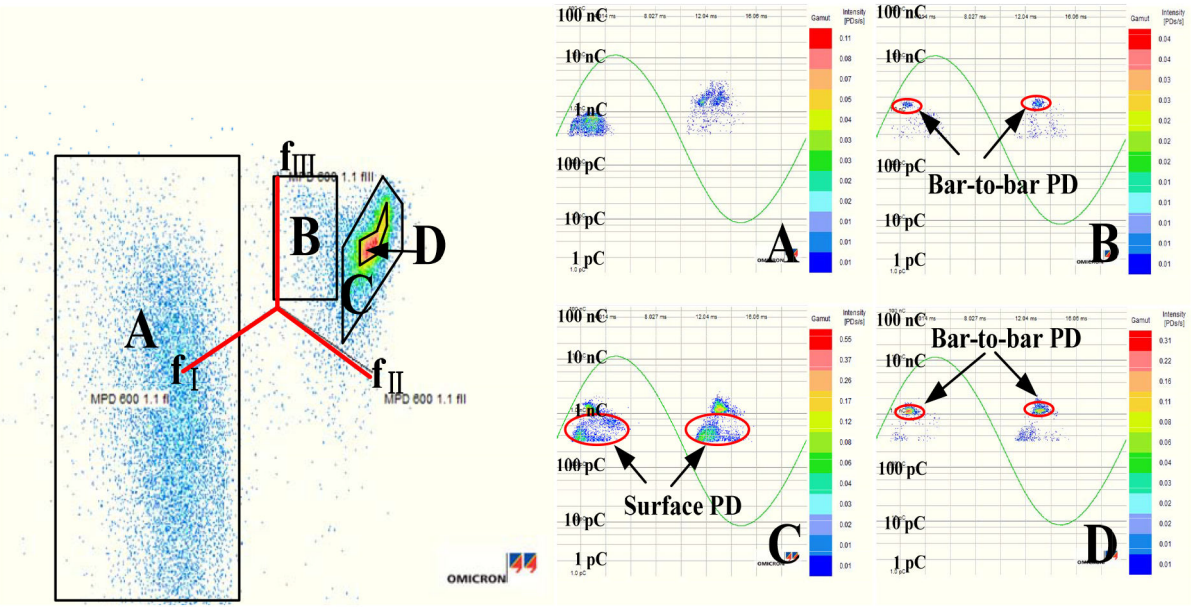


**Fig. 14** *PD distribution and its identification measured at 80°C and RH of 95% under the voltage 9.0 kV*

**Table 3** PD parameters extracted from PRPD patterns at RH = 60% and 10.0 kV. (corona PD: C, bar-to-bar PD: B, surface PD: S)

| | $Q_{peak}$ | $Q_{Avg}$ | DRR | $P_{Dis}$ | PD Types |
|---|---|---|---|---|---|
| 80°C | 10,800 pC | 7302 pC | 1082 PDs/s | 9288 μW | C, B, S |
| 20°C | 1124 pC | 594.2 pC | 264.1 PDs/s | 1174 μW | C, B |
| ratio | 9.6 | 12.3 | 4.1 | 7.9 | — |

**Table 4** PD parameters extracted from PRPD patterns at 20°C and 10 kV

| | $Q_{peak}$ | $Q_{Avg}$ | DRR | $P_{Dis}$ |
|---|---|---|---|---|
| 40% | 3989 pC | 1588 pC | 586.9 PDs/s | 4222 μW |
| 95% | 560.1 pC | 311.5 pC | 15.05 PDs/s | 47.66 μW |
| ratio | 7.1 | 5.1 | 39.0 | 88.6 |

**Table 5** PD parameters extracted from PRPD patterns at 10 kV and different RH and temperature

| | $Q_{peak}$ | $Q_{Avg}$ | DRR | $P_{Dis}$ |
|---|---|---|---|---|
| 20°C, 40% | 3989 pC | 1588 pC | 586.9 PDs/s | 4222 μW |
| 80°C, 95% | 3487 pC | 1955 pC | 413.2 PDs/s | 4491 μW |
| ratio | 1.1 | 0.8 | 1.4 | 0.9 |

discharges are very rare and hard to identify, and this condition is more serious at room temperature, while bar-to-bar discharge and surface discharge are relatively easy to identify, as shown in Figs. 13 and 14.

## 5 Conclusions

This paper built the experimental model including the three most common types of end-winding discharges. The development process and pattern identification of multiple simultaneous PD sources were studied. The experimental results revealed that humidity and temperature have a great influence on the end-winding discharge development and PD identification. Conclusions can be summarised as follows:

(i) Generally, the three types of end-winding discharges are simultaneously present under applied high voltage and/or high temperature. The bar-to-bar discharge gives a characteristic PRPD pattern with better symmetry in both voltage half cycles, while corona discharge and surface discharge show a conspicuous asymmetry.

(ii) PDs are influenced by the experiment temperature and humidity. The PDs can be promoted in higher temperature but can also be suppressed with the increase of RH. The corona discharge is very hard to be detected when RH exceeds 80% and the surface discharge is in the majority when RH is higher than 80%. Besides, the discharge energy may be the same even if the experimental conditions differ considerably.

(iii) When the three types of end-winding discharges are present simultaneously, the surface discharge shows the largest amplitude. In addition, PDs are relatively easy to identify under the condition of high temperature and/or low RH.

In our experiment, we found that the end-winding discharge is much more complicated and it is hard to identify each type of discharge from the complex PRPD pattern. By now, we can understand some development rules of end-winding discharge under different temperature and RH, as well as identify some parts of PDs from the complex PRPD pattern. Nevertheless, we are still not able to accurately quantify all of these discharges and analyse the proportion of each discharge in a complex PRPD pattern. In order to solve these problems, further research is being performed in our lab.


This is an open access article published by the IET and CEPRI under the Creative Commons Attribution License (http://creativecommons.org/licenses/by/3.0/)

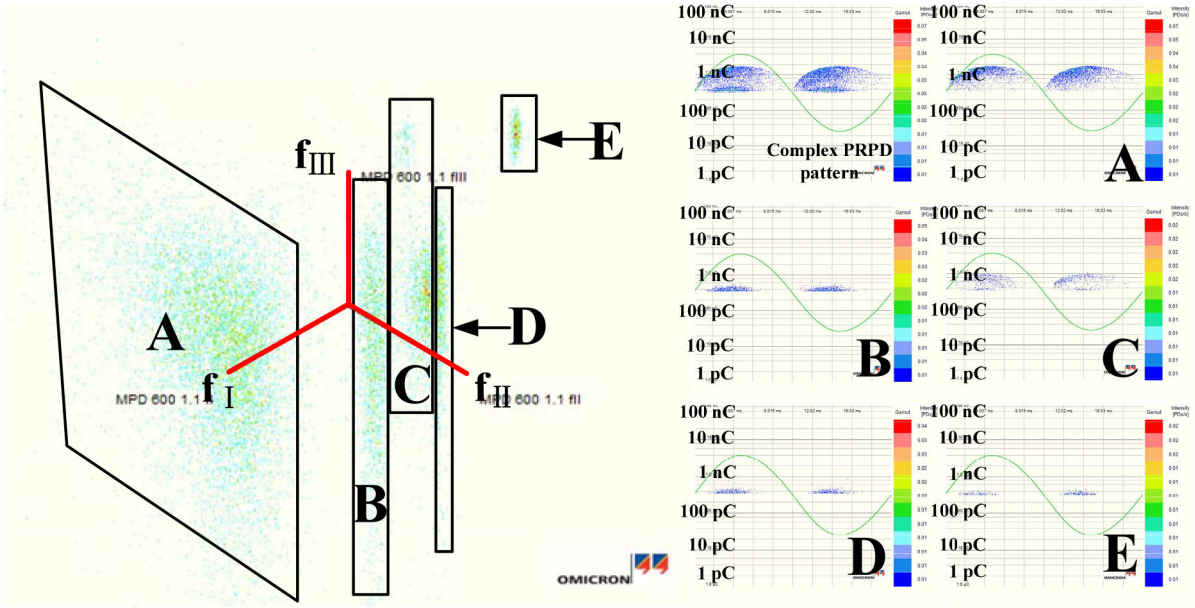


**Fig. 15** *Complex PRPD pattern and its PDs identification measured at 200°C and 6 kV*

## 6 Acknowledgments

The authors wish to express their deepest gratitude to the financial supports of the State National Natural Science Foundation (Nos. 51377113, 51577123 and U1510112), which ensured the successful completion of the experiment.

## 7 References

[1] Stone, G., Culbert, I., Boulter, E., *et al.*: '*Electrical insulation for rotating machines: design, evaluation, aging, testing, and repair*' (Wiley-IEEE Press, USA, 2014, 2nd edn.)

[2] Stone, G., Stranges, M., Dunn, D.: 'Recent developments in IEEE and IEC standards for off-line and on-line partial discharge testing of motor and generator stator windings'. Petroleum and Chemical Industrial Technologies Conf., San Francisco, USA, 2014, pp. 79–84

[3] Chuanyang, L., Jiancheng, S., Ailiang, K.: 'PD patterns of stator windings by in-factory experiment on a 10 kV motor'. Proc. IEEE Int. Symp. Electrical Insulation Material, Niigata, Japan, 2014, pp. 168–171

[4] Stone, G., Wu, R.: 'Examples of stator winding insulation deterioration in new generators'. Int. Conf. Properties and Applications Dielectric Materials, Harbin, China, 2009, pp. 180–185

[5] Hudon, C., Bélec, M., Lévesque, M.: 'Study of slot partial discharges in air-cooled generators', *IEEE Trans. Dielectr. Electr. Insul.*, 2008, **15**, (6), pp. 1675–1690

[6] Jiancheng, S., Chuanyang, L., Lingyan, L., *et al.*: 'Slot discharge pattern of 10 kV induction motor stator coils under condition of insulation degradation', *IEEE Trans. Dielectr. Electr. Insul.*, 2013, **20**, (6), pp. 2091–2098

[7] Janani, H., Kordi, B.: 'Towards automated statistical partial discharge source classification using pattern recognition techniques', *High Volt.*, 2018, **3**, (3), pp. 162–169

[8] Lévesque, M., David, É., Hudon, C., *et al.*: 'Contribution of humidity to the evolution of slot partial discharges', *IEEE Trans. Dielectr. Electr. Insul.*, 2012, **19**, (1), pp. 61–75

[9] Ailiang, K., Muqin, T., Jiancheng, S., *et al.*: 'Slot partial discharge characteristics under electro-thermal aging of 10 kV motor stator windings'. Int. Conf. Properties Applications Dielectric Materials, Xi'an, China, 2018, pp. 517–520

[10] Nair, R., Vishwanath, S., Rao, N.: 'Identification of slot discharges in rotating machine insulation system using variable frequency PD measurement', *High Volt.*, 2018, **3**, (3), pp. 179–186

[11] Lingyan, L., Ailiang, K., Jiancheng, S., *et al.*: 'Effect of water vapor on oil-contamination discharge of stator windings'. Int. Conf. Dielectrics, Montpellier, France, 2016, pp. 642–645

[12] Firuzi, K., Vakilian, M., Darabad, V.: 'A novel method for differentiating and clustering multiple partial discharge sources using S transform and bag of words feature', *IEEE Trans. Dielectr. Electr. Insul.*, 2017, **24**, (6), pp. 3694–3702

[13] Lévesque, M., David, É., Hudon, C., *et al.*: 'The need for PD quantification based on the type of discharge sources'. Electrical Insulation Conf., Baltimore, 2017, pp. 380–383

[14] Zhuo, M., Yang, Y., Martin, K., *et al.*: 'Fractal-based autonomous partial discharge pattern recognition method for MV motors', *High Volt.*, 2018, **3**, (2), pp. 103–114

[15] Hudon, C., Bélec, M.: 'Partial discharge signal interpretation for generator diagnostics', *IEEE Trans. Dielectr. Electr. Insul.*, 2005, **12**, (2), pp. 297–319

[16] Lingyan, L., Ailiang, K., Jiancheng, S., *et al.*: 'Influences of humidity and temperature on oil contamination discharge of HV motor stator windings', *IEEE Trans. Dielectr. Electr. Insul.*, 2016, **23**, (5), pp. 2695–2703

[17] Chuanyang, L., Jiancheng, S., Lingyan, L., *et al.*: 'Effects of vapor with different chemical properties on corona partial discharges of stator windings', *IEEE Trans. Dielectr. Electr. Insul.*, 2014, **21**, (3), pp. 964–972

[18] Ailiang, K., Muqin, T., Jiancheng, S., *et al.*: 'Contribution of electrical-thermal aging to slot partial discharge properties of HV motor windings', *Jour. Elect. Engin. Tech.*, 2019, **14**, (3), pp. 1287–1298

[19] Jitka, F., Thomas, A.: 'Identification and localization of PD-sources in power-transformers and power-generators', *IEEE Trans. Dielectr. Electr. Insul.*, 2017, **24**, (1), pp. 17–30

[20] IEEE guide for the measurement of partial discharge in AC electric machinery, IEEE Standard 1434-2014, 2014-11-03

[21] Breen, H., Gulski, E., Smit, J., *et al.*: 'The importance on generator operating conditions on PD data evaluation'. Int. Symp. Electrical Insulation, Boston, 2002, pp. 582–585

[22] Kuffel, E.: 'Electron attachment coefficients in oxygen, dry air, humid air and water vapour', *Proc. Phys. Soc.*, 1959, **74**, (3), pp. 287–308

[23] Chuanyang, L., Chuanjie, L., Geng, C., *et al.*: 'Field-dependent charging phenomenon of HVDC spacers based on dominant charge behaviors', *Appl. Phys. Lett.*, 2019, **114**, (20), p. 202904


This is an open access article published by the IET and CEPRI under the Creative Commons Attribution License (http://creativecommons.org/licenses/by/3.0/)